Effect of C_2H_2/N_2 partial pressure ratio on microstructure and mechanical properties of Ti-Al-Si-C-N coatings

Jiabin Gu[a], Liuhe Li[a,*], Hu Miao[a], Yi Xu[b,c], Ye Xu[a,*], Jianfei Sun[a], Xiulan Wang[d], Zhaohui He[d]

[a] School of Mechanical Engineering and Automation, Beihang University, Beijing, PR China
[b] School of Engineering Science, University of Chinese Academy of Science, Beijing, PR China
[c] Institute of Mechanics, Chinese Academy of Sciences, Beijing, PR China
[d] Aerospace Research Institute of Materials and Processing Technology, Beijing, PR China

ARTICLE INFO

ABSTRACT

Ti-Al-Si-C-N nanocomposite coatings were deposited on cemented carbide (WC-10 wt%, Co) substrates by reactive magnetron sputtering technique. The effect of C_2H_2/N_2 partial pressure ratio on element concentration, deposition rate, microstructure, cross-sectional morphology, hardness and tribological properties of the coatings were studied. The coatings were found to have a nanocomposite structure consisting of nanocrystallities (Ti,Al)(C,N) and amorphous phase. The coating's columnar crystals structure was restrained with the increase of C_2H_2/N_2 partial pressure ratio. The deposition rates and nanohardness of coatings firstly increased with the increase of C_2H_2/N_2 partial pressure ratio and reached their maximum values of 133 nm/min and 35 Gpa, respectively, at C_2H_2/N_2 partial pressure ratio of 1:2 before decreasing. The friction coefficient and wear rates of Ti-Al-Si-C-N coatings dramatically decreased with the increase of C_2H_2/N_2 partial pressure ratio and reached the lowest value of 0.17 and 1.1×10^{-6} mm^3/Nm, respectively, at C_2H_2/N_2 partial pressure ratio of 1:1.

1. Introduction

Due to the excellent properties such as high hardness, good wear resistance and chemical stability, TiN coatings as one of the protective hard coatings in cutting tools, dies and many mechanical components to improve their lifetime and performance [1–5]. However, one of the major the main drawbacks of TiN is its limited oxidation resistance (approximately 500 °C) [6].To overcome this problem, aluminum was alloyed to form a TiAlN nanocrystalline coating, which significantly improved the high temperature hardness and oxidation resistance up to 800 °C [7–10]. It has also been reported that incorporation of silicon in TiN coating can further improve hardness (> 40 GPa), oxidation resistance (> 800 °C) and wear resistance of the TiSiN coating due to the microstructure of nano-sized TiN crystals embedded in amorphous Si_3N_4 [11–15]. Therefore, the possibility of combining hard phases such as nanocrystalline TiAlN with improved oxidation resistance, with Si_3N_4 amorphous phase achieving superhardness, has allowed to constitute the TiAlSiN coating, which significantly increases the life time and performance of high-speed cutting tools [16–20].

Moreover, incorporating the carbon element has been found to significantly improve the tribological property of TiN-based coatings [21–28], which usually lack solid lubricating properties and exhibit relatively high friction coefficients (0.4–0.9) [29–32]. Hydrocarbon gases such as CH_4 and C_2H_2 are usually used as carbon source in preparing those coatings. Therefore, the partial pressure ratio between carbon-containing gas and N_2 becomes an important control parameter that affects the properties of resulting coatings. For example, Huang et al. [33] deposited $TiC_xN_{(1-x)}$ coatings by filtered arc and found that a significant increase in surface roughness, microhardness and wear resistance of the coatings with the increase of CH_4/N_2 gas flow rate ratio. Jang et al. [34] indicated that tribological property of $TiAlC_xN_{1-x}$ coatings remarkably improved with the increase of $CH_4/(CH_4 + N_2)$ gas flow rate ratio. Xie et al. [35] synthesized Ti-Al-Si-C-N coatings by multi-plasma immersion ion implantation with different C_2H_2/N_2 gas flow rate ratios and pointed out that a-C is found in the coating and acts as a solid lubricant decreasing frication and wear. Those results from previous studies indicated that the microstructure and properties of the TiN-based hard coatings are significantly dependent on the hydrocarbon/nitrogen partial pressure ratio. However, the effect of C_2H_2/N_2 partial pressure ratio on the microstructure and mechanical properties of the Ti-Al-Si-C-N coatings synthesized by reactive magnetron sputtering technique is still not clear.

In this study, Ti-Al-Si-C-N hard coatings were deposited by reactive magnetron sputtering technique with different C_2H_2/N_2 partial pressure

J. Gu et al.

1 Mass Flow Control

2 Vacuum Chamber

3 Cooling Water

4 Magnetron

5 Substrate

6 Holder

7 Turntable

8 High-voltage pulsed power
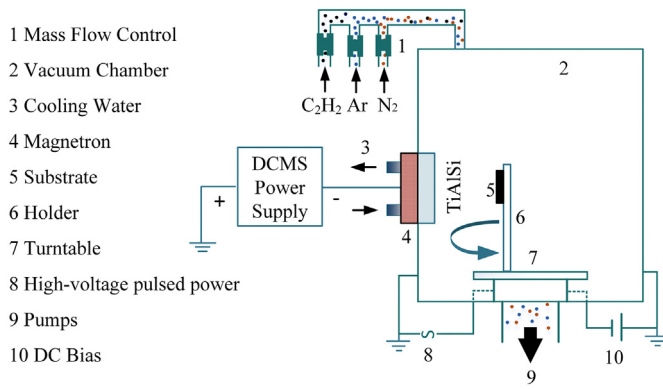
9 Pumps

10 DC Bias

Fig. 1. Schematic of the deposition apparatus.

ratios. The microstructure, morphology, nanoindentation hardness, and tribological properties of these coatings were studied as a function of C_2H_2/N_2 partial pressure ratio. The mechanism of how the C_2H_2/N_2 partial pressure ratio affects the coatings' microstructure and mechanical properties was discussed.

2. Experimental

2.1. Sample preparation

Ti-Al-Si-C-N coatings were prepared by reactive magnetron sputtering technique with different C_2H_2/N_2 partial pressure ratios. As shown in the schematic in Fig. 1, the rectangular ($12 \times 10 \text{ cm}^2$) $Ti_{0.64}Al_{0.3}Si_{0.06}$ targets were installed on the vacuum chamber wall. A detailed description of the system can be found in our earlier works [19, 20]. The deposition of Ti-Al-Si-C-N coatings was carried out in a mixture of high purity argon (99.999%), acetylene (C_2H_2 99.999%) and nitrogen (N_2 99.999%). The total working pressure and partial pressure of argon were kept constant at 0.8 Pa and 0.6 Pa, respectively. To study the effects of C_2H_2/N_2 partial pressure ratio, several independent mass flow controls were used to adjust C_2H_2/N_2 partial pressure ratio ranging from 0:1, 1:4, 1:3, 1:2 to 1:1. The cemented carbide (WC-10 wt% Co) was used as the substrate. Prior to deposition, all substrates were firstly mechanically polished, then ultrasonically cleaned, and etched by Ar ions directly to remove surface contaminants and the surface oxidation layer. The temperature of the substrates was kept constant at 150 °C during deposition. To enhance the adhesion of the deposited coating to the substrate, high-energy ion bombardment with average nitrogen ion energy of about 10 keV was applied for 20 min prior to the deposition. The sputtering parameters for Ti-Al-Si-C-N coatings are listed in Table 1. During deposition the substrate current stayed around 0.15 ± 0.01 A.

2.2. Characterization and evaluation of the coatings

The element content, cross-sectional morphology and thickness of coatings were measured by energy dispersive spectroscopy (EDS) and scanning electron microscope (SEM: Zeiss Supra 55). The crystalline structure of the coatings was characterized by X-ray diffraction (XRD:

D/Max 2500) with CuKα radiation in grazing-incidence mode (2°). Raman spectra were studied using a HR-800 Raman spectrometer operated at a laser wavelength of 532 nm to characterize the substructures of free carbon in the coatings. The hardness and Young's modulus of the coatings were obtained by nanoindentation (Nano-Indentor G200, Agilent) using continuous stiffness method (CSM). A maximum load of 50 mN was used to assure that the indentation depth was within the 5–10% of the coating thickness.

The tribological performance of coatings was evaluated by a HT-600 ball-on-disk tribometer using a load of 3.4 N. GCr15 bearing steel balls (6 mm diameter) were used as the counterparts. The tests were carried out at a sliding speed of 0.1 m/s under dry conditions at room temperature without lubricants. The sliding radius was 2 mm and the sliding time was 30 min. After the tests, wear tracks were investigated by a laser confocal scanning microscope (OLYMPUS OLS4100, Japan). Depth profiles across the width of the track, perpendicular to the sliding direction, were also calculated.

3. Results and discussion

3.1. Microstructure of the Ti-Al-Si-C-N coating

Table 2 shows the composition of the Ti-Al-Si-C-N coatings deposited with different C_2H_2/N_2 partial pressure ratios. Not surprisingly, as C_2H_2/N_2 partial pressure ratio increased, the C contents increase from 0 at.% to 59.48 at.% while N contents decrease from 37.95 at.% to 12.48 at.%. Meanwhile, the Ti, Al and Si contents also decrease correspondingly. However, the Ti, Al and Si relative content ratio in the coating is approximately 5.7:4.3:1, which is remains basically unchanged.

The cross-sectional morphologies of Ti-Al-Si-C-N coatings with different C_2H_2/N_2 partial pressure ratios were observed by SEM and the results were illustrated in Fig. 2. The thickness of the Ti-Al-Si-C-N coatings with the C_2H_2/N_2 partial pressure ratio of 0:1, 1:4, 1:3, 1:2, and 1:1 are 2.65, 2.95, 3.4, 4.0, and 3.0 μm, respectively. As shown in Fig. 2a, the columnar crystal structure is clearly seen in coatings deposited at C_2H_2/N_2 partial pressure ratio of 0:1. As C_2H_2/N_2 partial pressure ratio increased to 1:4, the columnar crystal structure is still visible, as shown in Fig. 2b. However, the length and the diameter of the columns both decrease comparing to the TiAlSiN coating shown in Fig. 2b. In the coating deposited with the C_2H_2/N_2 partial pressure ratio of 1:3, columnar crystal structure disappears and the coating shows a granular structure instead, as shown in Fig. 2c. As C_2H_2/N_2 partial pressure ratio further increased to 1:2, neither columnar crystal structure nor granular structure can be seen, and the coating exhibits a densified microstructure with a smooth cross-section, as shown in Fig.2d. This densified microstructure is consistent with the nanocomposite structure found in previous studies [36]. Finally, when C_2H_2/N_2 partial pressure ratio increased to 1:1, the cross-section of the deposited coating shows an amorphous like morphology, as shown in Fig. 2e. It is indicated that with the increase of C_2H_2/N_2 partial pressure ratio, the columnar crystal growth is restrained. This is likely due to the incorporation of the amorphous carbon or amorphous Si_3N_4, located at the grain boundary, can hinder the migration of grain boundary [28].
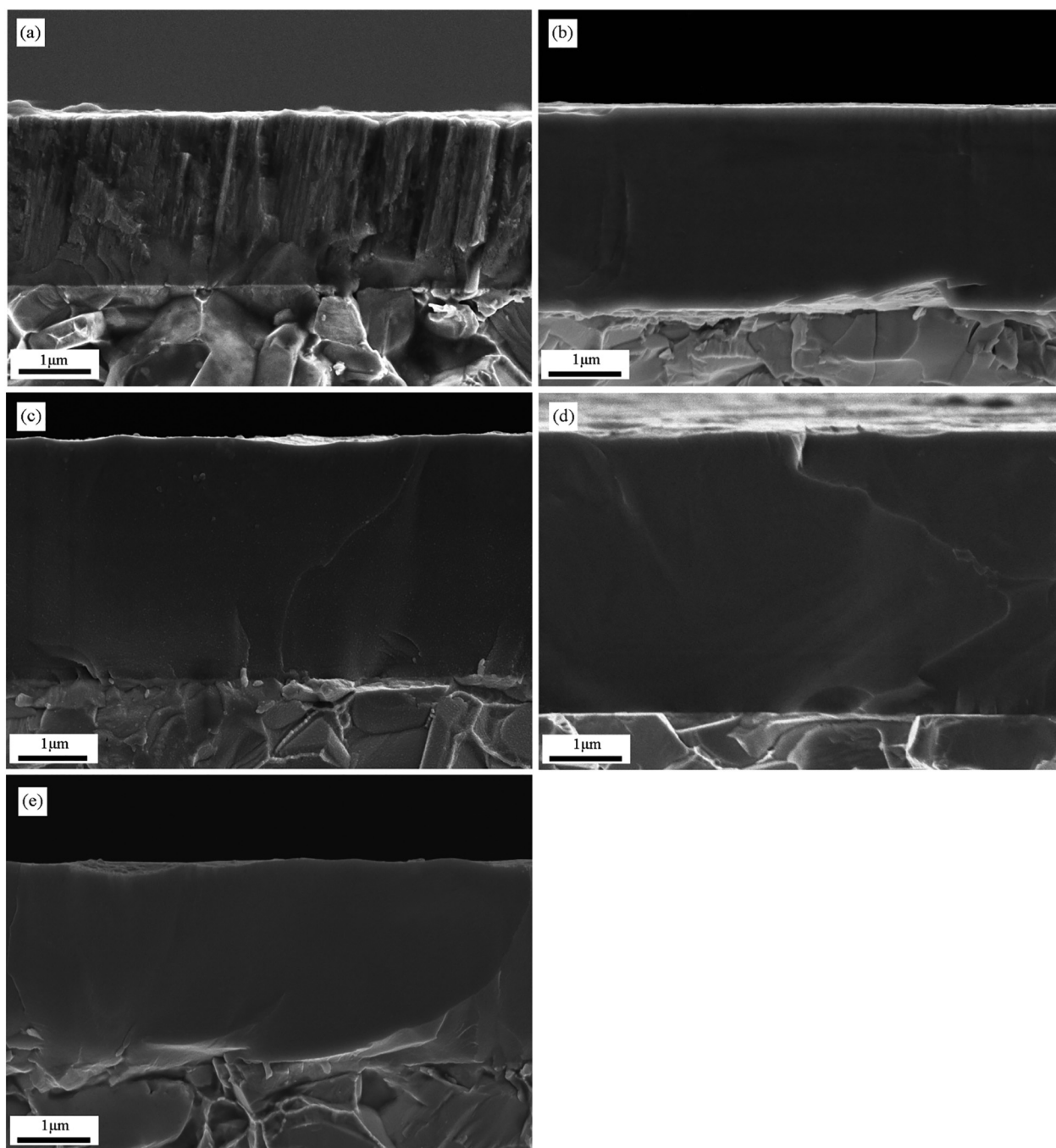
Fig. 3 presents the deposition rates of Ti-Al-Si-C-N coatings as a function of C_2H_2/N_2 partial pressure ratio. When C_2H_2/N_2 partial

Table 1
Details of deposition parameters.

Sample	Target-substrate distance (cm)	Substrate bias (V)	Temperature (°C)	P_{C2H2}/P_{N2}	P_{Ar} (Pa)	Working pressure (Pa)	Target current (A)
0: 1	8	−100	150	0/1	0.6	0.8	2
1: 4	8	−100	150	1/4	0.6	0.8	2
1: 3	8	−100	150	1/3	0.6	0.8	2
1: 2	8	−100	150	1/2	0.6	0.8	2
1: 1	8	−100	150	1/1	0.6	0.8	2

Table 2
Composition of Ti-Al-Si-C-N coatings.

Sample	Element composition (at.%)				
	Ti	Al	Si	C	N
0:1	32.03 ± 0.20	24.43 ± 0.15	5.59 ± 0.06	0	37.95 ± 0.39
1:4	29.28 ± 0.31	22.25 ± 0.28	5.17 ± 0.10	14.57 ± 0.12	28.73 ± 0.56
1:3	28.98 ± 0.45	19.94 ± 0.26	4.96 ± 0.19	18.20 ± 0.25	27.92 ± 0.95
1:2	25.94 ± 0.50	18.99 ± 0.31	4.52 ± 0.09	23.61 ± 0.25	26.94 ± 0.42
1:1	14.13 ± 0.19	11.49 ± 0.22	2.42 ± 0.03	59.48 ± 0.28	12.48 ± 0.43

Fig. 2. Cross-sectional morphologies of Ti-Al-Si-C-N coatings with different C_2H_2/N_2 partial pressure ratios: (a) 0:1 (b) 1:4 (c) 1:3 (d) 1:2 (e) 1:1.
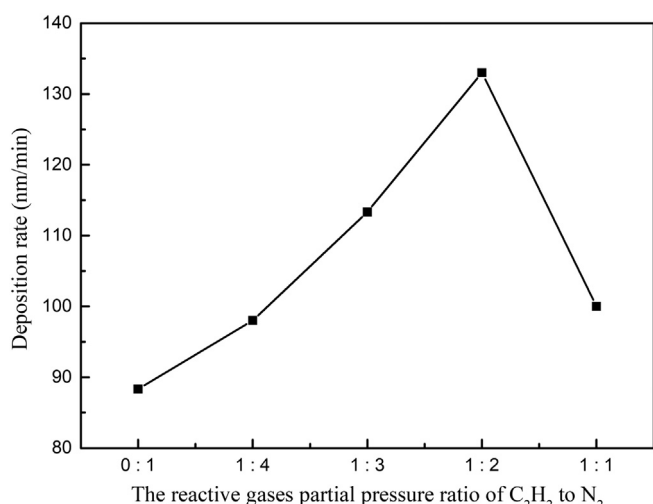
J. Gu et al.

Fig. 3. Deposition rates of Ti-Al-Si-C-N coatings as a function of the C_2H_2/N_2 partial pressure ratio.

pressure ratio increased from 0:1 to 1:2, the deposition rate dramatically increased from 88.33 nm/min to about 133 nm/min. This phenomenon can be explained as follows: The ionization energy for N_2 and C_2H_2 are 15.58 eV [37] and 11.403 eV [38, 39], respectively. Therefore, C_2H_2 are more apt to be ionized than N_2. In other word, C element is more active during the deposition. Carbon-containing particles are more likely to settle down and form carbon-based coatings on the substrate. As a result, the deposition rates increased with the increase of C_2H_2/N_2 partial pressure ratio. With the further increasing C_2H_2/N_2 partial pressure ratio, the deposition rate decreased. This is due to the fact that TiAlSi targets were partial covered with amorphous carbon or even carbide, which in turn reduced the amount of atoms and ions sputtered from the targets, leading to the occurrence of poisoning phenomenon [7]. Those results indicated that the deposition rate of Ti-Al-Si-C-N coatings depended not only on the discharge parameters but also on the C_2H_2/N_2 partial pressure ratio. Similar results also were reported in Refs [40].

Fig. 4 shows the XRD patterns of the Ti-Al-Si-C-N coatings with different C_2H_2/N_2 partial pressure ratios, and the standard peaks of TiN, TiC, and substrate WC are tagged. The diffraction peaks of Si_3N_4, SiC, TiSi crystalline phases were not discovered, indicating that the silicon atoms likely exist in the form of amorphous silicon nitride (a-Si_3N_4) and
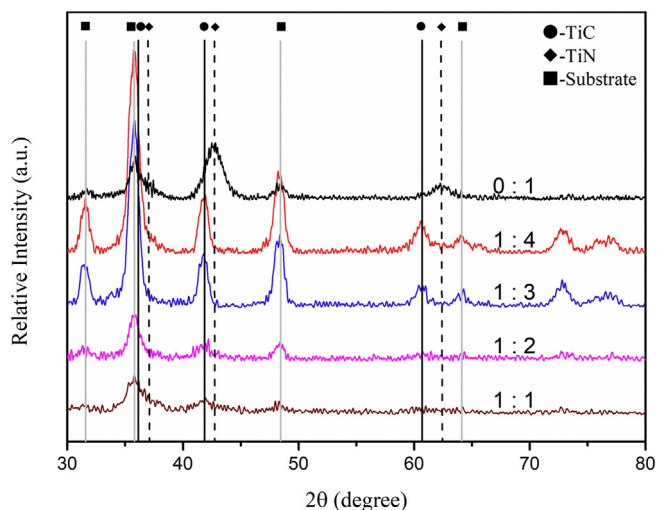

Fig. 4. X-ray diffraction pattern of Ti-Al-Si-C-N coatings with different C_2H_2/N_2 partial pressure ratios.
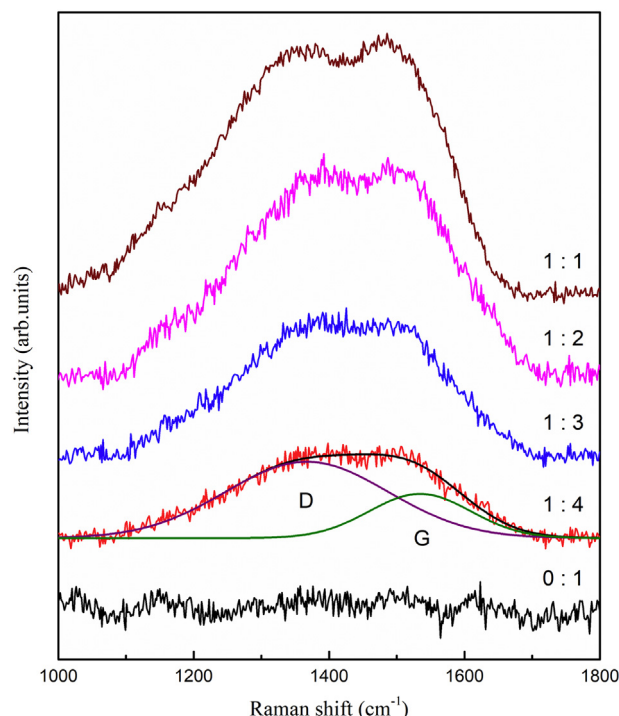

Fig. 5. Raman spectra of Ti-Al-Si-C-N coatings with different C_2H_2/N_2 partial pressure ratios.

silicon carbide (a-SiC) or are incorporated in the fcc lattice, or both [41–46]. With an increase of C_2H_2/N_2 partial pressure ratio, the position of one of the major peaks evidently shifts from TiN (42.6°) to TiC (41.9°), indicating gradual replacement of TiN phase by TiC phase. This is consistent with the results in Table 2 showing that a decrease of N content with the increase of C_2H_2/N_2 partial pressure ratio. Those results clearly show that more and more N atoms in the Ti-N structure are being replaced by C atoms with the increase of C_2H_2/N_2 partial pressure ratio [33, 47].

To further understand the detailed structure of Ti-Al-Si-C-N coatings, the Raman spectra of the coatings were measured and the results are shown in Fig. 5. For the film deposited at C_2H_2/N_2 partial pressure ratio of 0:1, no Raman signal corresponding to amorphous carbon-based material was discovered. When C_2H_2/N_2 partial pressure ratio increased, a broad asymmetric band between 1000 and 1800 cm^{-1} was present, which indicates the formation of amorphous carbon structure. Additionally, it can be clearly seen that as C_2H_2/N_2 partial pressure ratio increased the intensity of the amorphous carbon signal also increased. In order to perform a more detailed analysis, the broad asymmetric spectra were fitted by two Gaussian distributions. The band centered at about 1350 cm^{-1} corresponding to the D band of the disordered structure and the other band centered at about 1580 cm^{-1} related to the G band for the graphite structure [48–50]. The integrated intensity ratio of the D and G band (I_D/I_G) can be correlated with the sp^3/sp^2 ratio. The I_D/I_G ratio of Ti-Al-Si-C-N coatings as a function of C_2H_2/N_2 partial pressure ratio is shown in Fig. 6. When C_2H_2/N_2 partial pressure ratio exceeded 1:4, the I_D/I_G value stayed around 4 ± 0.2, indicating the existence of a large portion of amorphous carbon phase consisted of sp^2 (graphite-like) bonds in the Ti-Al-Si-C-N coatings [51]. In summary, these results suggest that the Ti-Al-Si-C-N coatings have a nanocomposite structure composing of nanocrystallities (Ti,Al)(C,N) and amorphous phase. It should be noted, however, that the diffraction peaks of AlN crystalline phases with hexagonal closed packed structure were not observed from the XRD results, which indicated that the aluminum atoms are incorporated in the fcc lattice or exist as amorphous aluminum nitride (a-AlN), or both [52–54]. Further confirmation
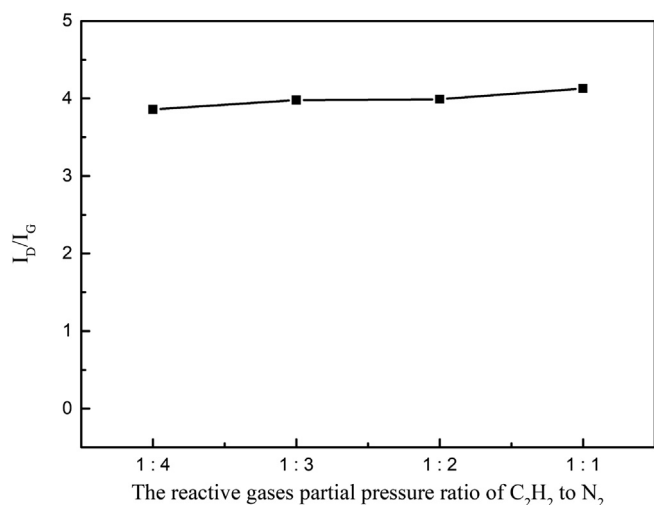
Fig. 6. I_D/I_G ratios of Ti-Al-Si-C-N coatings as a function of the C_2H_2/N_2 partial pressure ratio.

Fig. 8. Friction coefficients curves of the Ti-Al-Si-C-N coatings with different C_2H_2/N_2 partial pressure ratios.

of this interpretation would require an imaging with Transmission Electron Microscopy (TEM), which will be conducted in our follow-up study.

3.2. Mechanical properties of the Ti-Al-Si-C-N coatings

Fig. 7 shows the effect of C_2H_2/N_2 partial pressure ratio on the hardness and Young's modulus of Ti-Al-Si-C-N coatings. As C_2H_2/N_2 partial pressure ratio increased, the hardness evidently increased and reached a maximum value of 35 GPa at C_2H_2/N_2 partial pressure ratio of 1:2. This can be explained that with the increase of C_2H_2/N_2 partial pressure ratio, more and more carbon atoms replace nitrogen atoms to form Ti(C,N) solid solution. Because of the influence of the solid solution effect, the hardness of the coatings is expected to increase. Other possible reasons would be due to the nanocomposite structure of the nanocrystalline separated by amorphous phase mechanism would be the nanocomposite structure where the nanocrystalline (Ti,Al)(C,N) separated by amorphous phase (a-Si₃N₄, a-SiC and carbon). The nanocomposite structure can refine grain and hinder the movement of dislocations by the ideal interaction between nanocrystallites and the amorphous phase [36]. The highest hardness of Ti-Al-Si-C-N coatings demonstrates an optimal ratio of amorphous/nanocrystals and an appropriate C_2H_2/N_2 partial pressure ratio (1:2 in this work). With the further increasing C_2H_2/N_2 partial pressure ratio, the ideal interaction between nanocrystallites and the amorphous phase no longer exists, and therefore the hardness decreased [29]. The Young's modulus of Ti-
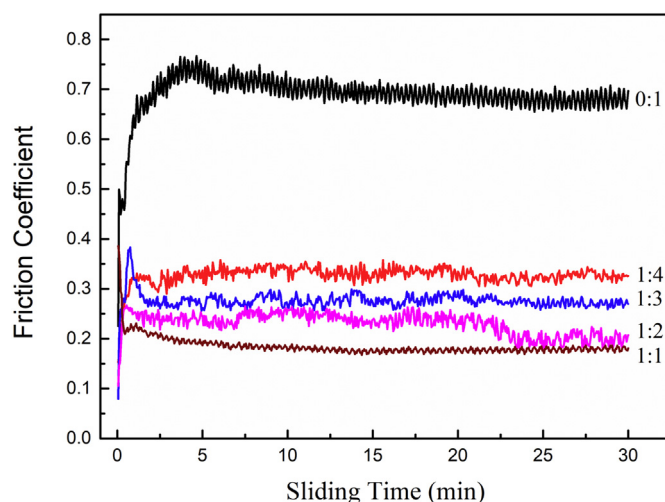
Al-Si-C-N coatings is also shown in the same plot in Fig. 7. As C_2H_2/N_2 partial pressure ratio increased from 0:1 up to 1:4, Young's modulus, which is sensitive to density and atomic structure of coating [55], sharply decreased from 360 GPa to 290 GPa. This decrease could be explained by the different chemical compositions in those coatings. When the carbon atoms accompanied with hydrogen were introduced in to the coatings, flexible sp^1, sp^2, sp^3 sites were formed, coinciding with the D and G peak seen in Fig. 5. As C_2H_2/N_2 partial pressure ratio increased from 1:4 up to 1:2, Young's modulus dramatically increased and reached the maximum values of 380 GPa. This result would be attributed to the densification of Ti-Al-Si-C-N coatings with a-Si₃N₄ and a-C filling the open structure of Ti(C,N) grain boundary. When C_2H_2/N_2 partial pressure ratio changed from 1:2 to 1:1, the Young's modulus renewedly decreased again. It may be due to the increase of volume fraction of a-Si₃N₄ and a-C, which has a relatively lower atomic density than that of the crystalline Ti(C,N) phase [29].

The friction coefficients curves of the Ti-Al-Si-C-N coatings with different C_2H_2/N_2 partial pressure ratios are shown in the in Fig. 8. It can be seen that the Ti-Al-Si-C-N coatings generally have a lower friction coefficient, comparing with that of TiAlSiN coatings. With the increase of C_2H_2/N_2 partial pressure ratio, the friction coefficients of the Ti-Al-Si-C-N coatings decreased remarkably from about 0.3 to approximately 0.17. The reduction of friction coefficient is due to the formation of the new amorphous phase (a-C) (supported by the results from Raman spectroscopy) and the increase of carbon content in the coatings. Amorphous carbon is known to exhibit low friction coefficient and can be used to as a solid lubricant [56]. A higher value of I_D/I_G ratio corresponds to higher sp^2 content in materials with good solid self-lubricant properties. Therefore, with the increase of C_2H_2/N_2 partial pressure ratio, the amount of a-C increases, which in turn, decreases the friction coefficients of the coatings.

To investigate the wear resistance of the Ti-Al-Si-C-N coatings against GCr15 balls, the surface morphologies of the wear tracks were observed by laser confocal scanning microscope. The 3D images and 2D cross-sectional profiles of the wear tracks on the Ti-Al-Si-C-N coatings with different C_2H_2/N_2 partial pressure ratios are shown in Fig. 9, in which the maximum wear depth was marked. It is important to point out that the scale ranges of the Y-axis in Fig. 9(a) are much larger than that in the other figures due to the very width of the wear track. The wear track on TiAlSiN coatings is much wider (about 430 μm), and deeper (2.7 μm) when compared with that on Ti-Al-Si-C-N coatings. The maximum depths of the wear track for the coatings with the C_2H_2/N_2 partial pressure ratio of 0:1, 1:4, 1:3, 1:2, and 1:1 are 2.7, 2.5, 2.1, 1.2, and 0.7 μm, respectively. Fig. 10 shows the wear rates of the Ti-Al-Si-C-
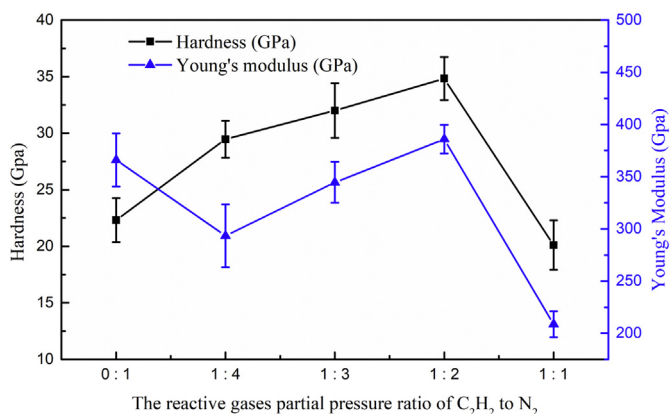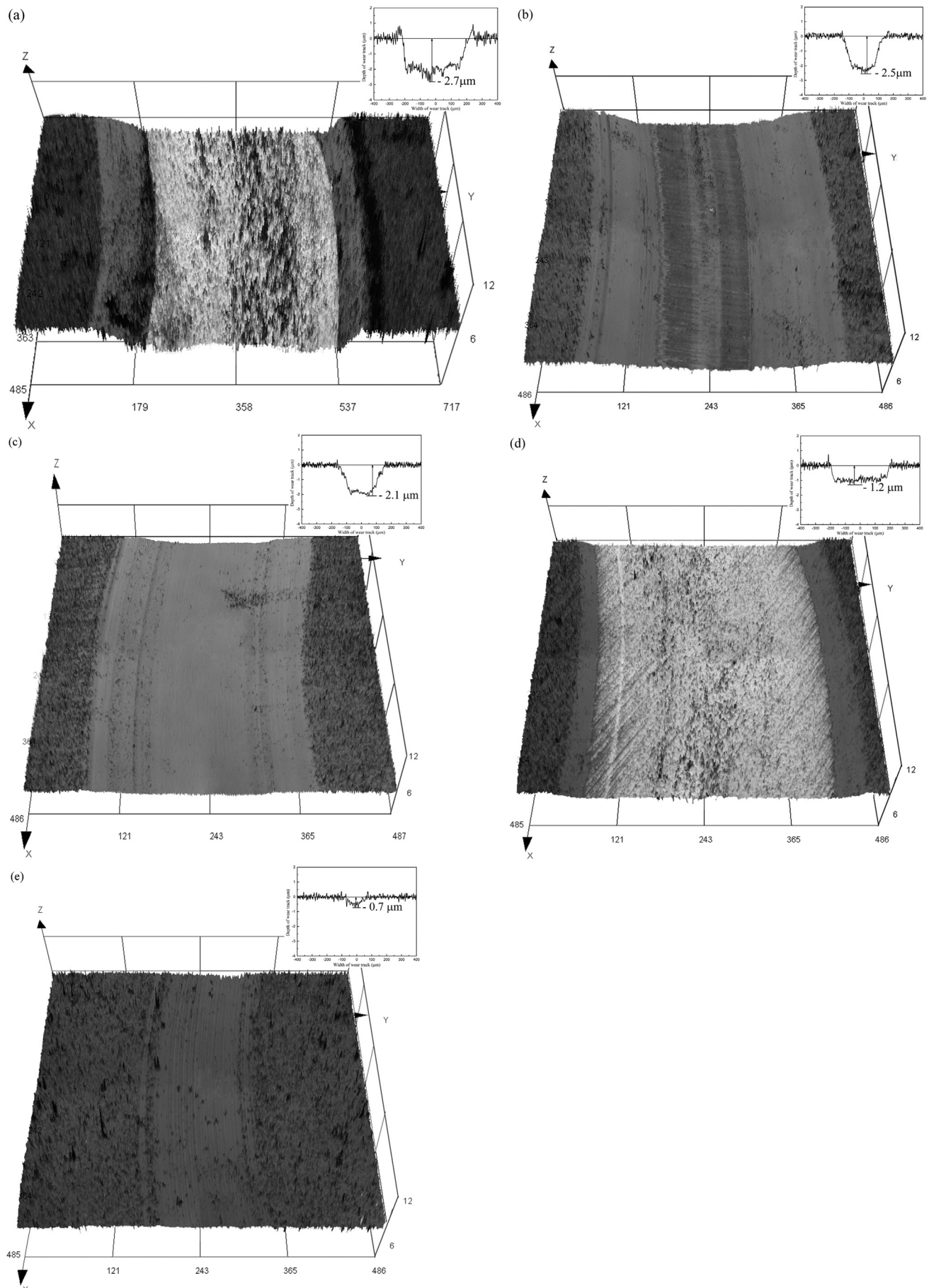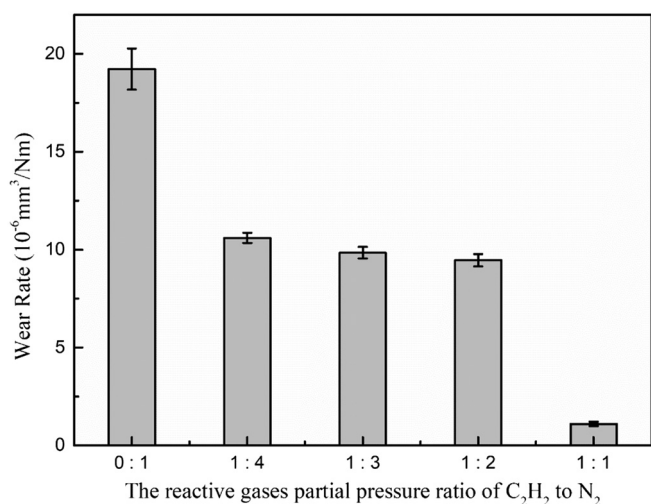

Fig. 7. Effect of C_2H_2/N_2 partial pressure ratio on the hardness and Young's modulus of Ti-Al-Si-C-N coatings.

(a)

(b)

(c)

(d)

(e)

(caption on next page)

Fig. 9. The 3D images and 2D cross-sectional profiles of the wear tracks on the Ti-Al-Si-C-N coatings with different C_2H_2/N_2 partial pressure ratios: (a) 0:1 (b) 1:4 (c) 1:3 (d) 1:2 (e) 1:1.

Fig. 10. Wear rates of the Ti-Al-Si-C-N coatings with different C_2H_2/N_2 partial pressure ratios.

N coatings with different C_2H_2/N_2 partial pressure ratios. The wear rates were calculated from the cross-sectional profiles of wear tracks. For TiAlSiN coatings, the wear rate is about 1.92×10^{-5} mm^3/Nm. As the C_2H_2/N_2 partial pressure ratio increased from 0:1 to 1:4, the wear rate reduced by 43% to 1.02×10^{-5} mm^3/Nm. A further increase of the C_2H_2/N_2 partial pressure ratio to 1:1 leads to a gradual decrease in the wear rate to 1.1×10^{-6} mm^3/Nm. Those results indicate a continuous improvement of wear resistance of the coatings with an increase of C_2H_2/N_2 partial pressure ratio.

The wear resistance is strongly dependent on the microstructure, hardness of the coating, friction coefficient, and lubricated phase [56]. For TiAlSiN coatings, the combination of the relatively looser microstructure, low hardness of the coating, high friction coefficient, and absence of the lubricated phase in the coating contribute to the high wear rate. When C_2H_2/N_2 partial pressure ratio increased from 0:1 to 1:2, the combination of densified microstructure, increase of the hardness and formation of a lubricated phase (a-C) in the Ti-Al-Si-C-N coatings resulted a remarkable decrease in the wear rate. With a further increase of C_2H_2/N_2 partial pressure ratio, the reduction in the friction coefficient causes a gradual decrease in the wear rate.

4. Conclusion

In this study, Ti-Al-Si-C-N coatings were prepared by reactive magnetron sputtering technique with different C_2H_2/N_2 partial pressure ratios. The effect of C_2H_2/N_2 partial pressure ratio on coatings' microstructure and mechanical properties has been investigated. From XRD and Raman studies it could be suggested that the coatings were composed of a mixture of nanocrystallities (Ti,Al)(C,N) and amorphous phase. With the increase of C_2H_2/N_2 partial pressure ratio, the columnar crystals structure in the coatings was restrained, resulting a densified microstructure. The deposition rate dramatically increased from 88.33 nm/min to about 133 nm/min as the C_2H_2/N_2 partial pressure ratio increased from 0:1 to 1:2, then decreased with the further increase of C_2H_2/N_2 partial pressure ratio. As C_2H_2/N_2 partial pressure ratio increased, the hardness remarkably increased and reached a maximum value of 35 GPa at C_2H_2/N_2 partial pressure ratio of 1:2 before decreasing. Moreover, both the friction coefficients and wear rates sharply decreased as C_2H_2/N_2 partial pressure ratio increased. The lowest friction coefficient and wear rate were 0.17 and

1.1×10^{-6} mm^3/Nm. This behavior would be attributed to the densified microstructure, the significant increase of the hardness and the formation of a lubricated phase (a-C) in the Ti-Al-Si-C-N coatings. Our comprehensive study on the effect of C_2H_2/N_2 provides insights in further improving the properties of Ti-Al-Si-C-N coatings.

References

[1] Z. Wang, D. Zhang, P. Ke, X. Liu, A. Wang, Influence of substrate negative bias on structure and properties of TiN coatings prepared by hybrid HIPIMS method, J. Mater. Sci. Technol. 31 (2015) 37–42.

[2] L.W. Ma, J.M. Cairney, M.J. Hoffman, P.R. Munroe, Effect of coating thickness on the deformation mechanisms in PVD TiN-coated steel, Surf. Coat. Technol. 204 (2010) 1764–1773.

[3] F. Jiang, T.F. Zhang, B.H. Wu, Y. Yu, Y.P. Wu, S.F. Zhu, F.J. Jing, N. Huang, Y.X. Leng, Structure, mechanical and corrosion properties of TiN films deposited on stainless steel substrates with different inclination angles by DCMS and HPPMS, Surf. Coat. Technol. 292 (2016) 54–62.

[4] G. Ma, L. Wang, H. Gao, J. Zhang, T. Reddyhoff, The friction coefficient evolution of a TiN coated contact during sliding wear, Appl. Surf. Sci. 345 (2015) 109–115.

[5] M. Stoiber, E. Badisch, C. Lugmair, C. Mitterer, Low-friction TiN coatings deposited by PACVD, Surf. Coat. Technol. 163 (2003) 451–456.

[6] M. Wittmer, J. Noser, H. Melchior, Oxidation kinetics of TiN thin films, J. Appl. Phys. 52 (1981) 6659–6664.

[7] S. PalDey, S.C. Deevi, Single layer and multilayer wear resistant coatings of (Ti,Al) N: a review, Mater. Sci. Eng. A 342 (2003) 58–79.

[8] Y.H. Yoo, D.P. Le, J.G. Kim, S.K. Kim, P.V. Vinh, Corrosion behavior of TiN, TiAlN, TiAlSiN thin films deposited on tool steel in the 3.5 wt.% NaCl solution, Thin Solid Films 516 (2008) 3544–3548.

[9] P.H. Mayrhofer, A. Hörling, L. Karlsson, J. Sjölén, T. Larsson, C. Mitterer, L. Hultman, Self-organized nanostructures in the Ti-Al-N system, Appl. Phys. Lett. 83 (2003) 2049–2051.

[10] O. Knotek, W.D. Münz, T. Leyendecker, Industrial deposition of binary, ternary, and quaternary nitrides of titanium, zirconium, and aluminum, J. Vac. Sci. Technol. A 5 (1987) 2173–2179.

[11] S. Vep Ek, S. Reiprich, A concept for the design of novel superhard coatings, Thin Solid Films 268 (1995) 64–71.

[12] S. Li, J. Deng, G. Yan, H. Cheng, Effects of nitrogen flowrates on properties of TiSiN coatings deposited by arc ion plating combining with medium-frequency magnetron sputtering, Int. J. Refract. Met. Hard Mater. 42 (2014) 108–115.

[13] S. Veprek, R.F. Zhang, M.G.J. Veprek-Heijman, S.H. Sheng, A.S. Argon, Superhard nanocomposites: origin of hardness enhancement, properties and applications, Surf. Coat. Technol. 204 (2010) 1898–1906.

[14] Y.X. Xu, L. Chen, Z.Q. Liu, F. Pei, Y. Du, Improving thermal stability of TiSiN nanocomposite coatings by multilayered epitaxial growth, Surf. Coat. Technol. 321 (2017) 180–185.

[15] Y. Xu, L. Li, X. Cai, P.K. Chu, Hard nanocomposite Ti-Si-N films prepared by DC reactive magnetron sputtering using Ti–Si mosaic target, Surf. Coat. Technol. 201 (2007) 6824–6827.

[16] D. Philippon, V. Godinho, P.M. Nagy, M.P. Delplancke-Ogletree, A. Fernández, Endurance of TiAlSiN coatings: effect of Si and bias on wear and adhesion, Wear 270 (2011) 541–549.

[17] S. Veprek, H.D. Männling, P. Karvankova, J. Prochazka, The issue of the reproducibility of deposition of superhard nanocomposites with hardness of ≥50 GPa, Surf. Coat. Technol. 200 (2006) 3876–3885.

[18] Y. Tanaka, N. Ichimiya, Y. Onishi, Y. Yamada, Structure and properties of Al-Ti-Si-N coatings prepared by the cathodic arc ion plating method for high speed cutting applications, Surf. Coat. Technol. 146–147 (2001) 215–221.

[19] Q. Ma, L. Li, Y. Xu, X. Ma, Y. Xu, H. Liu, Effect of Ti content on the microstructure and mechanical properties of TiAlSiN nanocomposite coatings, Int. J. Refract. Met. Hard Mater. 59 (2016) 114–120.

[20] Q. Ma, L. Li, Y. Xu, J. Gu, L. Wang, Y. Xu, Effect of bias voltage on TiAlSiN nanocomposite coatings deposited by HiPIMS, Appl. Surf. Sci. 392 (2017) 826–833.

[21] Y. Wang, J. Li, C. Dang, Y. Wang, Y. Zhu, Influence of carbon contents on the structure and tribocorrosion properties of TiSiCN coatings on Ti6Al4V, Tribol. Int. 109 (2017) 285–296.

[22] J. Li, Y. Wang, Y. Yao, Y. Wang, L. Wang, Structure and tribological properties of TiSiCN coating on Ti6Al4V by arc ion plating, Thin Solid Films 644 (2017) 115–119.

[23] W. Tillmann, S. Momeni, Tribological development of TiCN coatings by adjusting the flowing rate of reactive gases, J. Phys. Chem. Solids 90 (2016) 45–53.

[24] S.J. Bull, D.G. Bhat, M.H. Staia, Properties and performance of commercial TiCN

coatings. Part 2: tribological performance, Surf. Coat. Technol. 163–164 (2003) 507–514.

[25] Q. Wang, F. Zhou, S. Gao, Z. Zhou, L.K. Li, J. Yan, Effect of counterparts on the tribological properties of TiCN coatings with low carbon concentration in water lubrication, Wear 328–329 (2015) 356–362.

[26] I. Endler, M. Höhn, M. Herrmann, H. Holzschuh, R. Pitonak, S. Ruppi, H.V. den Berg, H. Westphal, L. Wilde, Aluminum-rich TiAlCN coatings by low pressure CVD, Surf. Coat. Technol. 205 (2010) 1307–1312.

[27] R. Wei, C. Rincon, E. Langa, Q. Yang, Microstructure and tribological performance of nanocomposite Ti-Si-C-N coatings deposited using hexamethyldisilazane precursor, J. Vac. Sci. Technol. A 28 (2010) 1126–1132.

[28] C. Chang, T. Hsieh, Effect of C_2H_2 gas flow rate on synthesis and characteristics of Ti-Si-C-N coating by cathodic arc plasma evaporation, J. Mater. Process. Technol. 209 (2009) 5521–5526.

[29] I. Park, S.R. Choi, J.H. Suh, C. Park, K.H. Kim, Deposition and mechanical evaluation of superhard Ti-Al-Si-N nanocomposite films by a hybrid coating system, Thin Solid Films 447–448 (2004) 443–448.

[30] S. Ma, J. Procházka, P. Karvánková, Q. Ma, X. Niu, X. Wang, D. Ma, K. Xu, S. Veprek, Comparative study of the tribological behaviour of superhard nanocomposite coatings nc-TiN/a-Si3N4 with TiN, Surf. Coat. Technol. 194 (2005) 143–148.

[31] D. Yu, C. Wang, X. Cheng, F. Zhang, Microstructure and properties of TiAlSiN coatings prepared by hybrid PVD technology, Thin Solid Films 517 (2009) 4950–4955.

[32] C. Chang, J. Lee, M. Tseng, Microstructure, corrosion and tribological behaviors of TiAlSiN coatings deposited by cathodic arc plasma deposition, Thin Solid Films 517 (2009) 5231–5236.

[33] S.W. Huang, M.W. Ng, M. Samandi, M. Brandt, Tribological behaviour and microstructure of $TiC_xN_{(1-x)}$ coatings deposited by filtered arc, Wear 252 (2002) 566–579.

[34] C.S. Jang, J. Jeon, P.K. Song, M.C. Kang, K.H. Kim, Synthesis and mechanical properties of $TiAlC_xN_{1-x}$ coatings deposited by arc ion plating, Surf. Coat. Technol. 200 (2005) 1501–1506.

[35] Z.W. Xie, L.P. Wang, X.F. Wang, L. Huang, Y. Lu, J.C. Yan, Microstructure and tribological properties of diamond-like carbon and TiAlSiCN nanocomposite coatings, Surf. Coat. Technol. 206 (2011) 1293–1298.

[36] Y. Wang, L. Zhengxian, D. Jihong, H. Yunfeng, W. Baoyun, (Ti,Al,Si,C)N nanocomposite coatings synthesized by plasma-enhanced magnetron sputtering, Appl. Surf. Sci. 258 (2011) 456–460.

[37] C. Guo, M. Li, J.P. Nibarger, G.N. Gibson, Single and double ionization of diatomic molecules in strong laser fields, Phys. Rev. A 58 (1998) 4271–4274.

[38] S.L. Sorensen, O. Björneholm, I. Hjelte, T. Kihlgren, G. Öhrwall, S. Sundin, S. Svensson, S. Buil, D. Descamps, A.L. Huillier, J. Norin, C.G. Wahlström, Femtosecond pump-probe photoelectron spectroscopy of predissociative Rydberg states in acetylene, J. Chem. Phys. 112 (2000) 8038–8042.

[39] J.E. Reutt, L.S. Wang, J.E. Pollard, D.J. Trevor, Y.T. Lee, D.A. Shirley, Photoelectron spectroscopy and inferred femtosecond intramolecular dynamics of $C_2H_2^+$ and $C_2D_2^+$, J. Chem. Phys. 84 (1986) 3022–3031.

[40] J. Walkowicz, J. Smolik, K. Miernik, J. Bujak, Anti-wear properties of Ti(C,N) layers

deposited by the vacuum arc method, Surf. Coat. Technol. 81 (1996) 201–208.

[41] S. Vepr Ek, S. Reiprich, L. Shizhi, Superhard nanocrystalline composite materials: the TiN/Si3N4 system, Appl. Phys. Lett. 66 (1995) 2640.

[42] S. Carvalho, L. Rebouta, A. Cavaleiro, L.A. Rocha, J. Gomes, E. Alves, Microstructure and mechanical properties of nanocomposite (Ti,Si,Al)N coatings, Thin Solid Films 398 (2001) 391–396.

[43] F. Vaz, L. Rebouta, P. Goudeau, J. Pacaud, H. Garem, J.P. Rivière, A. Cavaleiro, E. Alves, Characterisation of $Ti_{1-x}Si_xN_y$ nanocomposite films, Surf. Coat. Technol. 133 (2000) 307–313.

[44] S. Veprek, New development in superhard coatings: the superhard nanocrystalline-amorphous composites, Thin Solid Films 317 (1998) 449–454.

[45] A. Niederhofer, P. Nesladek, H.D. Männling, K. Moto, S. Veprek, M. Jilek, Structural properties, internal stress and thermal stability of nc-TiN/a-Si3N4, nc-TiN/TiSix and nc-(Ti1−yAlySix)N superhard nanocomposite coatings reaching the hardness of diamond, Surf. Coat. Technol. 120 (1999) 173–178.

[46] J.H. Jeon, S.R. Choi, W.S. Chung, K.H. Kim, Synthesis and characterization of quaternary Ti-Si-C-N coatings prepared by a hybrid deposition technique, Surf. Coat. Technol. 188 (2004) 415–419.

[47] R.R. Manory, S. Mollica, L. Ward, K.P. Purushotham, P. Evans, J. Noorman, A.J. Perry, The effects of MEVVA ion implantation on the tribological properties of PVD-TiN films deposited on steel substrates, Surf. Coat. Technol. 155 (2002) 136–140.

[48] Y. Xu, L.H. Li, P.K. Chu, Deposition of diamond-like carbon films on interior surface of long and slender quartz glass tube by enhanced glow discharge plasma immersion ion implantation, Surf. Coat. Technol. 265 (2015) 218–221.

[49] M. Ramsteiner, J. Wagner, Resonant Raman scattering of hydrogenated amorphous carbon: Evidence for π-bonded carbon clusters, Appl. Phys. Lett. 51 (1987) 1355–1357.

[50] R.O. Dillon, J.A. Woollam, V. Katkanant, Use of Raman scattering to investigate disorder and crystallite formation in as-deposited and annealed carbon films, Phys. Rev. B 29 (1984) 3482–3489.

[51] H.J. Choe, S. Kwon, J. Lee, Tribological properties and thermal stability of TiAlCN coatings deposited by ICP-assisted sputtering, Surf. Coat. Technol. 228 (2013) 282–285.

[52] Z.J. Liu, P.W. Shum, Y.G. Shen, Hardening mechanisms of nanocrystalline Ti-Al-N solid solution films, Thin Solid Films 468 (2004) 161–166.

[53] F. Jose, R. Ramaseshan, S. Dash, T.S. Sundari, D. Jain, V. Ganesan, P. Chandramohan, M.P. Srinivasan, A.K. Tyagi, B. Raja, Significance of Al on the morphological and optical properties of $Ti_{1-x}Al_xN$ thin films, Mater. Chem. Phys. 130 (2011) 1033–1037.

[54] F. Li, Y. Lin, W. Chen, S.C. Kwon, M. Li, S. Zhang, Influence of Al/Ti atomic ratio on hard Al-TiCN films, Surf. Eng. 31 (2015) 919–922.

[55] D. Schneider, M.D. Tucker, Non-destructive characterization and evaluation of thin films by laser-induced ultrasonic surface waves, Thin Solid Films 290 (1996) 305–311.

[56] Y.H. Cheng, T. Browne, B. Heckerman, E.I. Meletis, Influence of the C content on the mechanical and tribological properties of the TiCN coatings deposited by LAFAD technique, Surf. Coat. Technol. 205 (2011) 4024–4029.